Acta Biomaterialia 212 (2026) 624–636

Contents lists available at ScienceDirect

Acta Biomaterialia

journal homepage: www.elsevier.com/locate/actbio

Full length article

Micellar co-delivery of KRAS-mutant inhibitors and TLR7/8 agonists synergizes targeted therapy and immunotherapy in lung cancer

Shiyu Miao [a,1], Yinping Sun [a,1], Yanyi Qu [a,1], Luying Zhu [a], Zhiyuan Zhong [a,b,*], Fenghua Meng [a,*]

[a] Biomedical Polymers Laboratory, College of Chemistry, Chemical Engineering and Materials Science, and State Key Laboratory of Radiation Medicine and Protection, Soochow University, Suzhou 215123, China
[b] College of Pharmaceutical Sciences, Soochow University, Suzhou 215123, China

ARTICLE INFO

Keywords:
KRAS-mutant cancers
Molecular targeted therapy
Immune activation
Nanomedicines
Cancer immunotherapy

ABSTRACT

KRAS-mutant lung cancers pose significant clinical challenges. Despite promising advance in covalent KRAS G12C inhibitors, many patients with G12C mutation reveal limited responses, due to rapid emergence of resistance and heterogeneous nature of KRAS mutations. Here, we report a reduction-sensitive micellar system for the codelivery of a KRAS G12C inhibitor (adagrasib, KI) and a TLR7/8 agonist (R848, TA) (mKITA), aiming to synchronize direct oncogenic signaling blockade with potent immune modulation within tumor microenvironment (TME). In KRAS G12C-mutant lung cancer LLC cells, mKITA displayed enhanced autophagy and apoptosis, inducing marked immunogenic cell death at an optimal KI/TA molar ratio of 8/1. This in turn, stimulated dendritic cell (DC) maturation, proinflammatory cytokine secretion, and robust T cell activation-manifesting as a pronounced in situ vaccine effect. In an orthotopic LLC model, systemic administration of mKITA brought about significant survival benefits, and remodeled the suppressive TME by depleting immunosuppressive MDSCs, Tregs and M2M, and recruiting effector immune subsets (DCs, IFN-γ^{+}CTLs, Th1). Notably, combination therapy with αPD-1 achieved 60% complete tumor eradication and long-term survival, accompanied by epitope spreading and humoral responses against both KRAS and WT1 antigens. These results suggest that mKITA is capable of enabling in situ vaccination and overcoming key barriers in KRAS-driven lung cancer. This strategy appears as a potential generalizable approach to orchestrate durable, multilayered antitumor immunity and address the clinical challenge of resistance and immunosuppression in KRAS-mutant lung cancers.

Statement of significance: KRAS-mutant lung cancer represents a major clinical challenge due to its resistance to both targeted kinase inhibition and immunotherapy. Current strategies provide limited efficacy because of tumor heterogeneity, rapid adaptation, and the immunosuppressive TME. We develop a reduction-sensitive micellar nanoplatform (mKITA) that enables synchronized, spatiotemporally controlled co-delivery of a KRAS G12C inhibitor and a TLR7/8 agonist. mKITA induces autophagy- and apoptosis-associated ICD, and primes APCs to trigger robust in situ T cell activation. This strategy effectively remodels immunosuppressive TME by depleting MDSCs while recruiting CTLs and Th1 cells. In orthotopic lung cancer models, combining mKITA with αPD-1 achieves complete tumor regression and long-term survival in 60% of mice. This strategy offers a clinically translatable nanomedicine to overcome resistance in KRAS-driven lung cancer.

1. Introduction

Lung adenocarcinoma is the most prevalent form of primary lung cancer that has kept as a leading cause of cancer-related mortality worldwide. Kirsten rat sarcoma viral oncogene (KRAS) mutations are a major driver in lung adenocarcinoma and are directly associated with tumor proliferation, metastasis and poor patient prognosis [1]. The inhibition of KRAS mutation is regarded as a straightforward strategy for these cancers [2], and the successful development of covalent KRAS G12C inhibitor adagrasib (MRTX849) represents a breakthrough therapy for advanced or metastatic lung cancers harboring KRAS G12C mutation [3,4]. Nevertheless, durable clinical responses remain limited

* Corresponding authors.
E-mail addresses: zyzhong@suda.edu.cn (Z. Zhong), fhmeng@suda.edu.cn (F. Meng).
[1] These authors contributed equally to this work.

https://doi.org/10.1016/j.actbio.2025.12.045
Received 2 September 2025; Received in revised form 1 December 2025; Accepted 23 December 2025
Available online 24 December 2025

and most patients experience only partial response, largely due to the emergence of drug resistance and inherent molecular heterogeneity among KRAS mutations [5,6].

Resistance mechanisms in KRAS-mutant cancers include reactivation of alternative signaling pathways and profound alterations within tumor microenvironment (TME) [5], both of which blunt the effects of targeted therapies. The therapeutic efficacy of covalent KRAS inhibitors could be modestly improved through combination strategies, such as with co-administration with MAPK-related pathway inhibitors or immune checkpoint inhibitors [7–9]. However, the immunosuppressive TME continues to impede both targeted and immune checkpoint blockade (ICB) therapies [10,11]. Toll-like receptor (TLR) agonists capable of inducing innate immune responses have gained great interests for modulating TME and potentiate anti-tumor immune responses [12]. Of note, TLR7/8 agonist R848 has shown clinical potential as a cancer immunotherapeutic, albeit with acute adverse effects when administered systemically [13,14]. Nanomedicines offer distinct advantages for the delivery of both molecularly targeted agents and immune adjuvants, including increased tumor selectivity, reduction of the off-target toxicities, and the capacity for precise control over drug ratios at the tumor site, thereby maximizing therapeutic synergy [15–17].

Here, we report the development of a reduction-sensitive micellar system (mKITA) for codelivery of KRAS G12C inhibitor (adagrasib, KI) and TLR7/8 agonist (R848, TA), aiming to synchronize direct oncogenic signaling blockade with potent immune modulation within TME for G12C-mutant LLC cancer (Scheme 1). We have reported previously that sub-30 nm micelles based on poly(ε-caprolactone-co-dithiolane trimethylene carbonate) show high tumor penetration and efficient delivery of small chemical drugs to different tumors [18,19]. mKITA was engineered to afford three critical features: (i) enhanced co-delivery of KRAS G12C inhibitor and TLR7/8 agonist to the tumor, (ii) maintenance of an optimal drug ratio *in vitro* and *in vivo*, which overcomes the pharmacokinetic inconsistency of free drug combinations, and (iii) amplification of both targeted therapy and immunotherapy-mediated anti-tumor effects. Intriguingly, our results have proven our concept that this dual-delivery approach not only augments autophagy and apoptosis in KRAS-mutant LLC cells but also significantly enhances ICD and specific immune activation, enabling potent in situ vaccine effects. Such nanosystem simultaneously targeting multiple pathways counteracts acquired resistance and achieves sustained tumor suppression, surpassing cytostatic effects of clinical inhibitors, thereby establishing a versatile platform for "targeted" immunotherapy against lung adenocarcinoma.

2. Experimental section

2.1. Fabrication and characterization of mKITA

KRAS G12C inhibitor (adagrasib, KI) and TLR7/8 agonist (R848, TA) coloaded micelles (mKITA) were formulated from copolymer PEG-P(CL-DTC) ($\bar{M}_n$ = 2.0-(1.0-1.2) kg/mol), KI and TA, of which the concentration of each stock solution was 200 mg/mL, 30 mM, and 16 mM in PEG-350, respectively. Typically, for preparing micelle coloaded with KI/TA at a molar ratio of 8/1 (denoted as mKITA 8/1), 10 μL PEG-P(CL-DTC), 15 μL KI, 3.75 μL TA solution, and 21.25 μL PEG-350 were mixed, and added to 950 μL of phosphate buffer (PB, pH 7.4, 10 mM) at 37°C under mild stirring for 10 min followed by overnight storage at 37°C. For Cy5-labeled mKITA, the preparation procedure was the same except that 0.5 wt.% Cy5-labeled PEG-P(CL-DTC) copolymer was premixed. The colloidal stability of micelles upon storage at various temperature (25

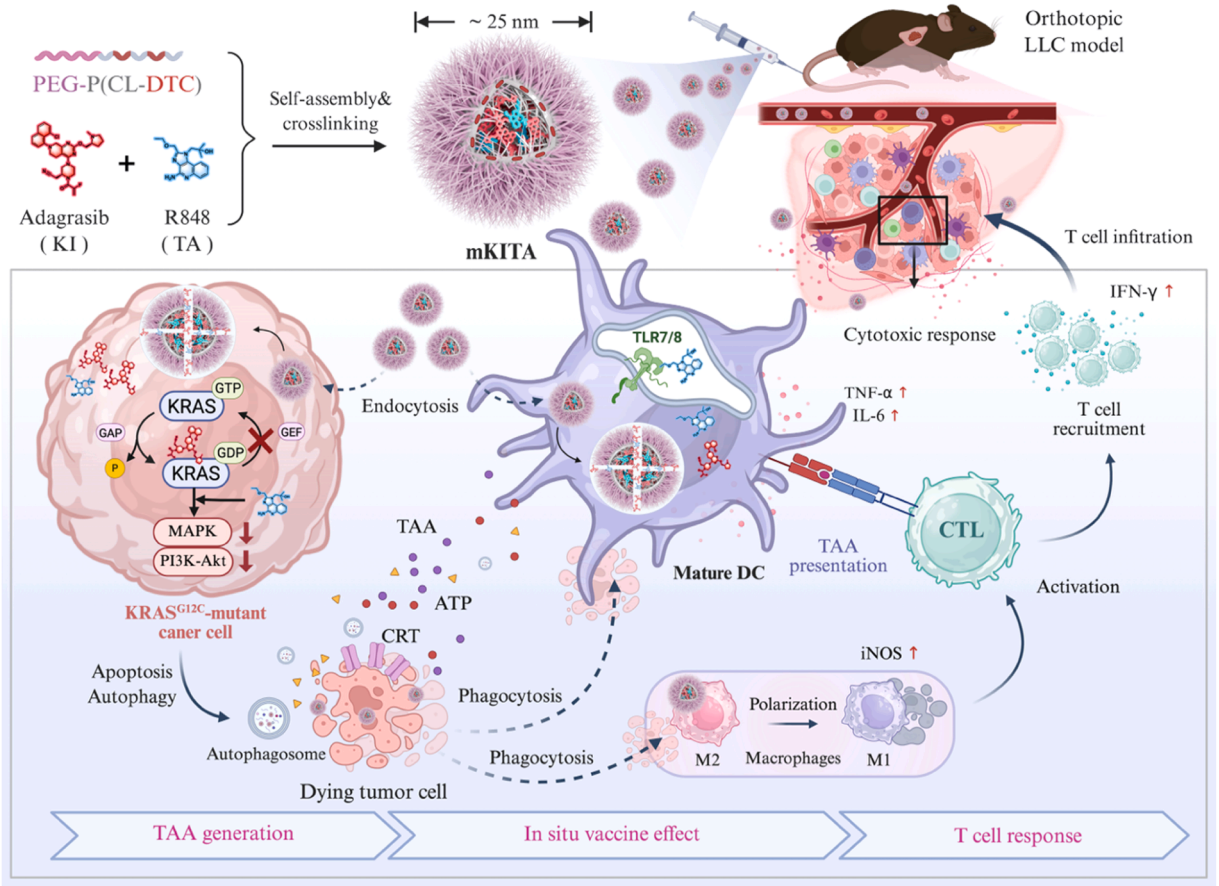

Scheme 1. KRAS G12C inhibitor (adagrasib, KI) and TLR7/8 agonist (R848, TA) coloaded micelle (mKITA) enhanced ICD via autophagy and apoptosis, enabling in situ vaccine effect and synergistic molecular targeted and immuno-therapy in orthotopic LLC model.

°C, 4 °C or -20 °C), in the presence of 10% FBS or GSH (10 mM) was investigated using DLS.

The release behavior of KI and TA from mKITA was studied using dialysis tubes in various media: PB (10 mM, pH 7.4) with or without 10 mM GSH, or PB (10 mM, pH 6.0, 10 mM GSH). Briefly, 0.5 mL of mKITA (0.5 mg/mL) was added to a dialysis tube and immersed in 15 mL of one of above medium under constant stirring (n = 3). At predetermined time points (1 to 24 h), 10 mL of dialysate was withdrawn for determination of KI and TA, and equal volume of fresh medium was respectively added. Dialysate was freeze-dried and re-dissolved in a mixed solution of acetonitrile/water containing 0.05% phosphoric acid (55/45, v/v) to measure the KI and TA concentration using HPLC.

2.2. Cytotoxicity studies of mKITA

LLC cells seeded in 96-well plates (3×10^3/well) were added with mKI, mTA, free KI, or free TA at various concentrations up to 50 μM, mKITA (1/1, 2/1, 4/1, 8/1, TA fixed at 15 μM) or PBS (n = 6). After 24 h incubation, MTT (5 mg/mL, 10 μL) was added to incubate for 4 h followed by washing, addition of 150 μL dimethyl sulfoxide (DMSO) and measurement of absorbance at 570 nm. Cell viability was determined by comparing the absorbance of samples to that of PBS group (as 100% viability) and plotted against drug concentration to derive half maximal inhibitory concentration (IC_{50}) and the combination index (CI) based on the equation: $CI = \frac{A}{C} + \frac{B}{D}$. A and B are the equivalent IC_{50} of KI and TA in mKITA, respectively; C and D are the IC_{50} of mKI and mTA, respectively. CI values below, equal to, or exceeding 1 signify the synergistic, additive or antagonistic effects, respectively.

2.3. Autophagy, apoptosis and ICD of LLC cells induced by mKITA

To investigate the autophagy, LLC cells were cultured in 6-well plates (8×10^5/well) overnight and incubated with mTA (5 μM), mKI (5 μM), mKITA (1/1, 1/0.125, KI: 5 μM) or PBS (n = 3). After 24 h, cells were lysed with RIPA for Western blot (WB) measurements. Proteins were isolated, purified and quantified before electrophoresis (30 μg) using standard procedure (PowerPac™). Band images were taken using chemiluminescence detector and quantified using ImageJ software (GAPDH as internal reference).

To study the apoptosis, LLC cells seeded in 12-well plates (1×10^5/well) were cultured overnight and incubated with mTA (5 μM), mKI (5 μM) or mKITA (1/1, 1/0.125, KI: 5 μM) for 24 h (n = 3). Cells were washed with PBS and treated with Annexin V-APC/7-AAD apoptosis kit before flow cytometry (FC) measurements and analysis.

To study ICD induction, LLC cells seeded in a 12-well plate (2×10^5/well) were cultured overnight and incubated with mTA (5 μM), mKI (5 μM), mKITA (1/1, 1/0.25, 1/0.125, KI: 5 μM) or PBS (n = 3). After 24 h, culture medium was taken to quantify ATP using an ATP assay kit. Cells were digested with trypsin, washed with PBS (2×), and incubated with blocking antibody (4 °C for 20 min) before 1 h incubation with anti-CRT antibody at room temperature. After washing (PBS, 3×), cells were incubated with Alexa Fluor 647 for 30 min and subjected to FC measurements.

2.4. Proliferation, migration and invasion of LLC cells

To assess the effect of mKITA on clone formation, LLC cells seeded in 6-well plates (800/well) were cultured overnight and incubated with mTA (5, 10 μM), mKI (5, 10 μM), or mKITA 8/1 (KI: 5, 10 μM). During 12-day culturing, medium was refreshed every 3 days. Cells were then fixed with 4% paraformaldehyde, stained with 1% crystal violet, washed, photographed and quantified semi-quantitatively using ImageJ.

To study the effect of mKITA on cell migration, LLC cells in 6-well plates (5×10^5/well) were cultured overnight to 80%-90% confluence, and a wound was created by gently scratching the cell layer with a 1-mL pipette tip. mTA (3 μM), mKI (3 μM) or mKITA 8/1 (KI: 3 μM) were rapidly added and incubate for 24 h (n = 3). Cells near the scratch were imaged under a microscope, and the width of the scratches was photographed and quantified semi-quantitatively using ImageJ.

The effect of mKITA on cell invasion was studied using a transwell model. On the insert, 200 μL 2.5% matrigel was plated, followed by hydration for 30 min, and LLC cells (5×10^4/mL, serum-free) were seeded on the gel, mTA (5 μM), mKI (5 μM), mKITA 8/1 (KI: 5 μM) or PBS were added to the upper chamber (n = 3). Meanwhile, 600 μL culture medium containing 20% FBS was added to the lower chamber to create a nutrient gradient. After incubation for 24 h, the inserts were taken, and cells on the lower side that penetrated through the matrigel and insert membrane were stained with 1% crystal violet, washed (PBS, 3×), and photographed and quantified semi-quantitatively using ImageJ.

To determine the effect of mKITA on genes related with proliferation, migration and invasion, LLC cells were cultured in 12-well plates (2×10^5/well) overnight and incubated with mTA (5 μM), mKI (5 μM), mKITA (1/1, 1/0.125, KI: 5 μM) or PBS (n = 3). After 24 h, cells were harvested, and total RNA was isolated and purified from cell lysate using RNA-easy Isolation Reagent. mRNA levels of KRAS, MAPK, AKT, EGFR, mTOR, VEGFA and MMP-9 were determined using qRT-PCR (GAPDH as internal reference, **Table S1**) and analyzed using 2-ΔΔCT method.

2.5. Competitive uptake of mKITA by co-cultured APCs and tumor cells

LLC cells (2×10^5 cells, DMEM) were stained with CM-Dil (10 μM) at 37 °C for 3 min and then at 4 °C for 15 min in the dark. Then LLC cells were mixed with BMDCs (or BMDMs) (2×10^5/well, RPMI-1640 medium) in 12-well plates overnight, and Cy5-labeled mKITA were added (8/1, KI: 3 μM, Cy5: 0.7 μM, n = 3). After co-incubation for 4 h, culture medium was taken for ELISA measurements of IL-6 and TNF-α, and all cells were collected and stained with FITC-αCD11c (or FITC-αCD11b for BMDMs) antibody and PE/Cy7-αCD86 antibody (4°C, 30 min) for FC measurement and analysis. Cells were stained with FITC-conjugated antibodies at 1:200 dilution and other antibodies at 1:400 dilution.

2.6. Activation of immune cells in the co-culture of APC and mKITA pretreated LLC cells

LLC cells and BMDCs co-culture: LLC cells (4×10^5/well, DMEM) were cultured in 12-well plates overnight and incubated with mKI (3 μM), mTA (3 μM), mKITA (1/1, 4/1, 8/1, TA: 3 μM, n = 3). After 5 h, culture medium was replaced with fresh medium to further cultured for 7 h. BMDCs (1×10^6/well, RPMI-1640 medium) were added to co-culture with LLC cells. After 8 h, medium was taken for ELISA measurements of IL-6, IL-12p70 and TNF-α, and cells were stained with Per/Cy5.5-αCD45, FITC-αCD11c, PE/Cy7-αCD86 and APC-αCD80 (4°C, 30 min) for FC measurement.

LLC cells and macrophage co-culture: LLC cells were treated as above, and IL-4 pre-treated (25 ng/mL, 24 h) RAW264.7 cells (5×10^5/well) were added to coculture (n = 3). After 8 h, cells were stained with FITC-αCD11b, PE-αF4/80 and APC-αiNOS for FC measurements.

LLC cells and splenic cells co-culture: LLC cells were treated as above, and fresh splenic cells (3×10^6/well, RPMI-1640 medium) from healthy C57 mice were added to coculture (n = 3). After 24 h, medium was taken for ELISA measurements of IFN-γ, and cells were stained with Per/Cy5.5-αCD45, APC-αCD3, PE-αCD4, FITC-αCD8a for FC measurements.

2.7. Anti-tumor efficacy of mKITA in orthotopic LLC-tumor bearing mice

All animal experiments performed in accordance with the Guidelines for Care and Use of Laboratory Animals of Soochow University (P.R. China) and approved by the Animal Ethics Committee of Soochow University (approval numbers: 202411A0090, 202412A0713, 202510A0362). Orthotopic LLC-tumor bearing mouse models (LLC

mice) were established by injecting 50 μL murine LLC cells (2.5×10^5) into the left lung of 8-week-old female C57BL/6J mice as previously reported . The tumor inoculation day was designated as day 0. From day 3, LLC mice were randomly grouped, and intravenously (i.v.) administered with 200 μL mKI, mTA, mKITA (KI: 16 mg/kg, TA: 1 mg/kg) or PBS on days 3, 5, 7, 9, 15 and 21 (n = 5). For combination therapy, αPD-1 (10 μg/mouse) was additionally i.v. injected on days 8, 10 and 16. Body weight and health status of the mice were monitored every 2 days. Survival were recorded upon either natural death or when body weight loss exceeding 15% was observed.

2.8. Immunological analysis

Orthotopic LLC mice were i.v. administered with 200 μL mTA, mKITA (KI: 16 mg/kg, TA: 1 mg/kg) or PBS on days 3, 7 and 9. For combination therapy, αPD-1 (10 μg/mouse) on days 8 and 10 (n = 5). On day 12, all mice were sacrificed to collect peripheral blood, lung, spleen and CLNs. Single-cell suspensions were prepared for determining DCs, macrophages, B cells, NK cells, T cells, Tregs, and MDSCs using FC (detailed in SI).

2.9. Statistical analysis

Data were analyzed using GraphPad Prism 8 software and presented as the mean ± SD. Differences among groups were evaluated using one-way ANOVA with Tukey's multiple comparison test, and survival curves were estimated using the Kaplan–Meier method with a log-rank comparison test. * $p < 0.05$ indicates significance, and ** $p < 0.01$, *** $p < 0.001$ and **** $p < 0.0001$ indicate high significance.

3. Results and discussion

3.1. Fabrication and characterization of mKITA

Biodegradable micelles capable of co-encapsulating KI (adagrasib) and TA (R848) (mKITA) were conveniently formulated from PEG-P(CL-DTC) in aqueous solution (**Fig. S1**). By adjusting KI/TA molar ratio (8/1, 4/1, 2/1, 1/1), we achieved uniform micellar sizes (23-26 nm) with high loading efficiencies (88%-95% for KI and 48%-58% for TA) (Fig. 1**A, Table S2**). Single drug-loaded micelles (mKI and mTA) exhibiting similar size and drug loading were used as controls. TEM image showed well-dispersed mKITA with a spherical morphology and an average size of ca. 26 nm. No critical micellar concentrations were detected for mKITA and Ms, indicating their crosslinked micellar cores (**Fig. S2**). The colloidal stability of mKITA was validated by their maintenance of structural integrity in 10% FBS as well as in PBS over two months stored at 4°C or -20°C with little drug leakage (< 6%) (Fig. 1A–C). Notably, mKITA demonstrated environmental responsiveness: in a circulation-mimicking condition (PB, pH 7.4), drug release was limited (< 20%), while over 70% of KI and TA were released under lysosomal and cytosol-mimicking reductive conditions (pH 6.0 or pH 7.4, 10 mM GSH) (Fig. 1**D**). Such selective release profile facilitates efficient intracellular delivery of KI to bind the G12C mutation site of KRAS and inhibit KRAS signaling, and TA to locally activate TLR7/8 within endosome of antigen presenting cells (APCs) [4,20], thereby maximizing tumor-targeted therapeutic synergy. This dual drug encapsulation strategy addresses a critical challenge in nanomedicine: maintaining optimal and synergistic drug ratios within tumors over sustained durations, which is essential for overcoming both pharmacokinetic mismatches and sub-optimal pharmacodynamics observed with conventional drug combinations [15,21]. Moreover, small micellar size further enhances the prospects for deep tumor penetration and broad intratumoral distribution, as recently reported in advanced nanoparticles for solid tumors [22].

3.2. In vitro cytotoxicity and synergistic effects of mKITA in LLC tumor cells

To evaluate antitumor activity, cytotoxicity assays were conducted on a KRAS G12C-mutant lung cancer LLC cells [23]. mKI exhibited higher cytotoxicity than free KI (Fig. 1**E**), possibly due to increased cellular uptake through endocytosis, consistent with studies emphasizing the role of carrier-mediated delivery in improving therapeutic index [21]. While neither mTA nor free TA was cytotoxic up to 50 μM, highlighting the requirement for combination therapy to achieve meaningful tumor cell death. Remarkably, in the same range of TA concentration, mKITA across various KI/TA molar ratios consistently exhibited enhanced cytotoxic activity over mKI alone, with a pronounced decrease in IC_{50}. The greatest synergy was observed at KI/TA = 1/0.125, achieving a low combination index (CI) of 0.47, indicating strong synergism [24] (Fig. 1**F**). This optimal ratio was used in subsequent studies if not otherwise stated. Mechanistically, this synergy may stem from R848-induced modulation of tumor cell stress through TLR activation, thereby sensitizing cells to KRAS pathway inhibition, as reported for R848-loaded nanoparticles [25].

To elucidate the cellular uptake mechanism [26], inhibitor studies revealed that mKITA internalization relied predominantly on dynamin- and caveolin- mediated endocytosis, but was independent of clathrin, micropinocytosis, or integrin-mediated processes (**Fig. S3**). This efficient intracellular delivery augmented KI bioavailability and thus provides a mechanistic basis for reduced dosing and the potential to delay or overcome acquired resistance, which is a major obstacle in the clinical management of KRAS-mutant tumors [5,27].

3.3. Autophagy, apoptosis and ICD of LLC cells induced by mKITA

Recent studies have demonstrated that KRAS pathway inhibition can trigger autophagy via mTOR/AMPK-dependent mechanisms in KRAS-mutant cancer, thereby modulating tumor cell fate and sensitizing cells to subsequent therapeutic stress [28]. Here, we assessed whether mKITA could enhance autophagic process in LLC cells and explored the underlying molecular interplay between autophagy and immunogenicity. WB analysis demonstrated marked upregulation of the autophagy marker LC3-II [29] and LC3-II/LC3-I ratios in both mKI and mKITA groups (Fig. 1**G-I**). Notably, mKITA at KI/TA = 1/0.125 induced the highest levels of LC3-II conversion, suggesting maximal autophagic flux at this combination. Increasing the proportion of TA (mKITA 1/1) resulted in a reduction in LC3-II/LC3-I ratio, an effect possibly attributed to an excessive TLR7/8 activation impairing autophagic processing via promoting the cytoplasmic accumulation of LC3-I. This pronounced autophagy observed in mKITA at the optimal ratio correlated with the highest cytotoxicity in LLC cells (Fig. 1**F**), directly linking intracellular stress pathways to tumoricidal outcomes. These results illustrate the importance of precise control over drug co-delivery ratios in nanomedicine-enabled combination therapies-a key concept highlighted in recent advanced materials research [21,30].

Parallel analysis of apoptotic responses demonstrated that, while mTA had minimal pro-apoptotic effects, mKI induced moderate apoptosis at therapeutically relevant concentrations (5 μM). Intriguingly, mKITA 1/0.125 further elevated apoptotic cell proportion, confirming synergistic induction of apoptosis (Fig. 1**J**). Conversely, a higher TA content dampened this effect, aligning with observations for autophagy. These data highlight delicate and ratio-dependent balance in autophagic and apoptotic pathways, both of which are increasingly recognized as drivers of immunogenic cell death (ICD) in the context of nanoparticle-enabled interventions [31–33]. Exploiting ICD is now considered as a central strategy for bridging effective tumor cytoreduction with robust antitumor immunity [34]. Accordingly, we investigated hallmark indicators of ICD, surface exposure of calreticulin (CRT) and release of ATP. Flow cytometry and biochemical assays showed that mKI alone significantly increased CRT surface translocation

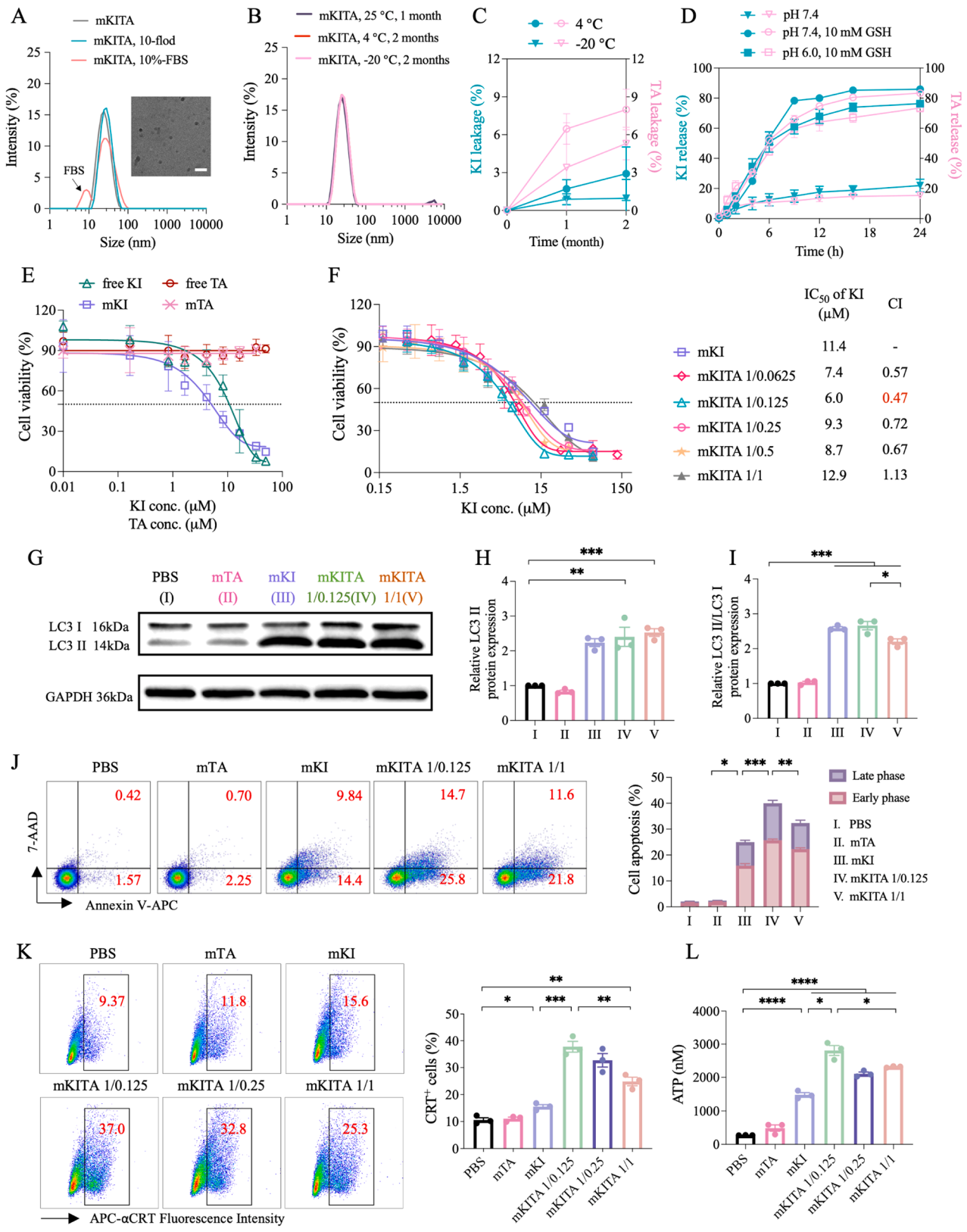

Fig. 1. Physicochemical properties of mKITA and the effects on LLC cells. (A) Size and size distribution mKITA after ten-fold dilution or addition of 10% FBS with TEM micrograph of mKITA as insert (scale bar: 100 nm). (B) Size distribution and (C) drug leakage after storage at 4°C or -20°C for 2 months (n = 3). (D) Drug release profiles of KI and TA under various conditions (n = 3). Viability of LLC cells treated with (E) free KI, free TA, mKI, mTA, and (F) mKITA at 24 h incubation (n = 6). (G) WB band images and (H) semi-quantification of the expression of autophagy marker LC3-II and (I) the LC3-I/LC3-II ratio (n = 3). (J) Apoptosis at 24 h incubation (n = 3). (K) Proportions of CRT^{+}cells and (L) concentrations of ATP in culture medium of LLC cells following 24 h incubation with mKITA (1/1, 1/0.25, and 1/0.125), mTA or mKI (n = 3). * $p < 0.05$, ** $p < 0.01$, *** $p < 0.001$ and **** $p < 0.0001$.

1.5-fold relative to PBS control, while mKITA 1/0.125 further synergistically increased this effect by 2.4-fold (Fig. 1**K**). Optimal combination additionally boosted extracellular ATP (Fig. 1**L**), a key immunostimulatory signal for DC activation.

Our data demonstrate that excessive R848 dosage compromises both autophagic and apoptotic cell death as well as ICD, emphasizing the necessity of an optimal intratumoral drug ratio for maximal immunologic benefit. This insight adds to the emerging paradigm that effective nano-immuno-therapies rely not only on co-delivery, but also on fine-tuning composition to harness the full therapeutic spectrum against immuno-suppressive tumors [21]. Our results indicate that mKITA is capable of orchestrating multiple immunologically-relevant cell death pathways. It induces autophagy and apoptosis, leading to enhanced ICD and the release of tumor-associated antigens (TAAs). TAAs are captured by APCs to activate systemic T-cell responses, thereby functioning as an in situ vaccine that elicits a personalized anti-tumor immune response in a minimally invasive manner. This provides a robust foundation for in vivo immune efficacy and TME modulation studies.

3.4. Inhibition of tumor cell proliferation, migration, and invasion by mKITA

Constitutive activation of KRAS and its downstream effectors drives uncontrolled clonal expansion, increased tumor aggressiveness, and metastatic progression in lung adenocarcinoma [35]. To elucidate the effect of mKITA on these malignant phenotypes, we conducted a series of functional *in vitro* assays using LLC cells. Long-term colony formation assays revealed that mKITA (1/0.125, KI: 5-10 μM) greatly suppressed clonogenic growth compared to mKI and mTA monotherapies, indicating potent anti-proliferative effects (Fig. 2**A**). These findings suggest a pronounced synergy derived from simultaneous delivery of the KRAS inhibitor and TLR7/8 agonist, echoing results from prior studies on the necessity of multi-pronged signaling inhibition for durable tumor growth suppression [25]. Wound healing and transwell invasion assays further demonstrated that mKITA significantly inhibited migration and invasive potential of LLC cells relative to controls (Fig. 2**B, C**). This is consistent with recent work highlighting the critical role of TME and cellular motility machinery in metastatic dissemination, and showcases the ability of nanomedicine platforms to disrupt these processes [36].

To unravel underlying mechanisms, qRT-PCR analysis was performed on key signaling nodes and metastatic mediators. mKITA 1/0.125 treatment led to robust downregulation of MAPK, AKT, KRAS, EGFR, and mTOR gene expression, drivers of tumor proliferation and survival, far surpassing the effects of either mKI or mTA alone (Fig. 2**D-H**). In addition, mKITA 1/0.125 significantly reduced the expression of VEGF and MMP-9 (Fig. 2**I, J**), two key mediators associated with angiogenesis and extracellular matrix remodeling, which are fundamental to metastatic potential. These results are supported by recent literature underscoring the necessity of multiplex pathway targeting to overcome the adaptative rewiring of oncogenic signaling networks in KRAS-mutant malignancies [8]. Interestingly, mKITA 1/0.125 demonstrated the most pronounced reduction of MAPK and AKT pathways compared to both monotherapies, while this formulation more considerably reduced the expression of other five genes that were upregulated by mTA, illustrating the benefit of the synergy of the two drugs at optimal ratio. Thus mKITA exerts comprehensive anti-tumor effects through multi-target and multi-pathway synergistic suppression of proliferative and metastatic circuits. Collective downregulation of these signaling pathways provides the molecular basis for enhanced autophagy, increased apoptosis, and pronounced ICD observed in LLC cells.

3.5. Direct immunomodulatory effects of mKITA on APCs

Given the complex cellular composition of TME, the direct impact of mKITA on key immune cells was first evaluated. BMDCs and M2-polarized BMDMs were incubated with mKITA, mKI, or mTA. Both mKITA and mKI exhibited good biocompatibility (cell viability > 85%) at KI concentrations below 10 μM (**Fig. S4A, B**), while mTA was not cytotoxic to both cells. Notably, while mKI and mTA promoted DC maturation, only mKITA 8/1 stimulated significantly elevated TNF-α secretion (**Fig. S4C, D**), paralleling recent findings that synergistic TLR7/8 stimulation and targeted therapy are required for maximal cytokine output [37]. R848-containing formulations (mTA and mKITA 8/1) increased macrophage polarization toward pro-inflammatory M1M (**Fig. S4E**). These data indicate the inherent flexibility of mKITA to directly prime APCs, laying the foundation for downstream immune activation.

3.6. mKITA triggered in situ-vaccine effects in tumor-immune co-culture models

To better recapitulate the cellular complexity of the tumor microenvironment, co-culture systems combining LLC tumor cells and immune cells were established. Flow cytometry assays illustrated that Cy5-labelled mKITA was simultaneously taken up by LLC cells and BMDCs, confirming high dual-positivity for APC markers and nanoparticle tracer (Fig. 3**A-C**). Notably, large proportions of $Dil^{+}CD11c^{+}$cells appeared, with > 80% Cy5 positivity within this subset, which was mainly ascribled to the interaction of mKITA-treated LLC cells with APCs. Functional assays demonstrated over 2-fold increase in DC maturation induced by mKITA relative to PBS group, showing possible direct TLR7/8 stimulation (Q3, ca. 60%) and tumor antigen-mediated cross-presentation (Q2, ca. 40%) (Fig. 3**D**). DC activation was accompanied by significant secretion of IL-6 and TNF-α (Fig. 3**E**), indicating robust pro-inflammatory signaling. BMDMs in co-culture with LLC cells showed enhanced phagocytosis of mKITA (Fig. 3**F**), yet R848-induced polarization toward the M1M subset was less pronounced than observed in DCs (Fig. 3**G, H**), likely reflecting TLR7/8 expression patterns [38]. Multi-SIM fluorescent imaging visualized dynamic interactions between nanoparticles, macrophages, and tumor cells, illustrating the real-time “in situ vaccination” process (**Fig. S5**).

Extending this observation, pre-conditioning LLC cells with mKITA prior to co-incubation with APCs amplified DC maturation and cytokine secretion in a KI dose-dependent manner (Fig. 4**B-F**). These mKITA-pretreated tumor cells also prime increased proportions of $iNOS^{+}$M1M (Fig. 4**G**), pointing to possible immune reprogramming within TME. Mechanistic dissection using autophagy inhibitors (CQ or HCQ) confirmed that mKITA-induced autophagy in tumor cells is requisite for maximal DC activation and maturation (Fig. 4**H, I**), reinforcing the notion that autophagy-dependent ICD is central to the immunogenicity of cell death and tumor antigen availability [32]. Moreover, mKITA treatment significantly upregulated MHC I expression on tumor cells, a key prerequisite for efficient T cell priming (**Fig. S6**), while this upregulation was significantly reduced upon autophagy inhibitor treatment. Pre-treated LLC cells, when co-cultured with murine splenocytes, resulted in enhanced T cell activation ($CD8^{+}$T, $CD4^{+}$T cells) and robust secretion of IFN-γ (Fig. 4**J-K**), further corroborating the potent “in situ vaccination” effect mediated by mKITA. Overall, our findings demonstrate that mKITA functions as a multifaceted immune activator, leveraging both direct stimulation of APCs and autophagy-dependent release of immunogenic tumor antigens to potently orchestrate DC and T cell responses, thus effectively acting as an “in situ vaccine”. This dual-pronged mechanism implies the potential of mKITA for precision targeted drug delivery and as a highly effective in situ tumor vaccines, uniquely synergizing with the complexities of TME.

3.7. Therapeutic activity of mKITA in orthotopic LLC mouse models

The antitumor activity of mKITA was evaluated in orthotopic LLC tumor mouse model. Mice received treatment of mKI, mTA, mKITA, or mKITA in combination with αPD-1 antibody (mKITA+αPD-1), and overall survival was monitored (Fig. 5**A**). All treatment regimens were

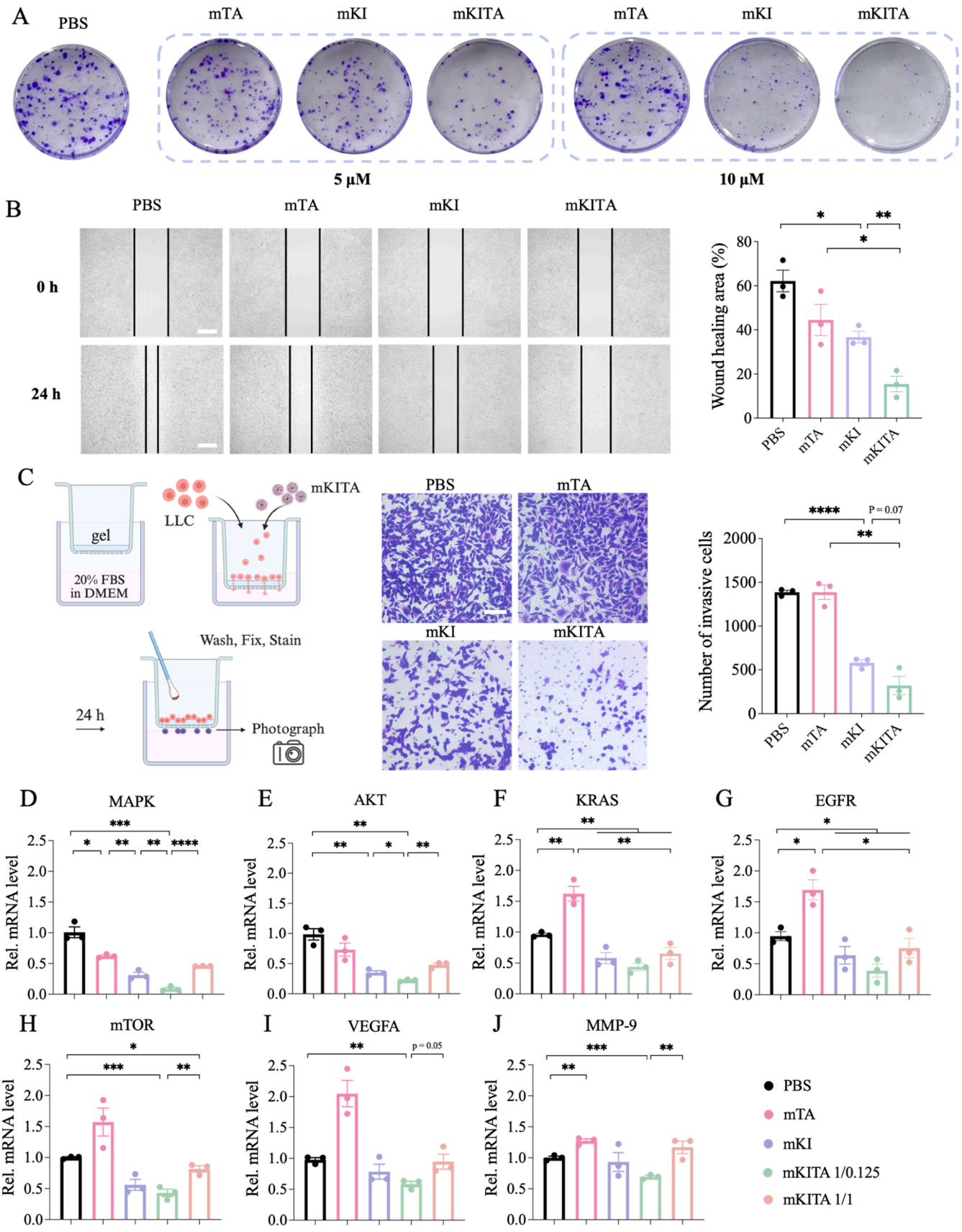

Fig. 2. Effect of mKITA on LLC cells. Inhibition of (A) clone formation, (B) migration (scale bar: 250 μm) and (C) invasion (scale bar: 100 μm) of LLC cells by mKITA, mTA or mKI (n = 3). qRT-PCR determination of mRNA expression of (D) MAPK, (E) AKT, (F) KRAS, (G) EGFR, (H) mTOR, (I) VEGFA, and (J) MMP-9 in LLC cells following 24 h incubation with mKITA, mTA or mKI (n = 3). * $p < 0.05$, ** $p < 0.01$, *** $p < 0.001$ and **** $p < 0.0001$.

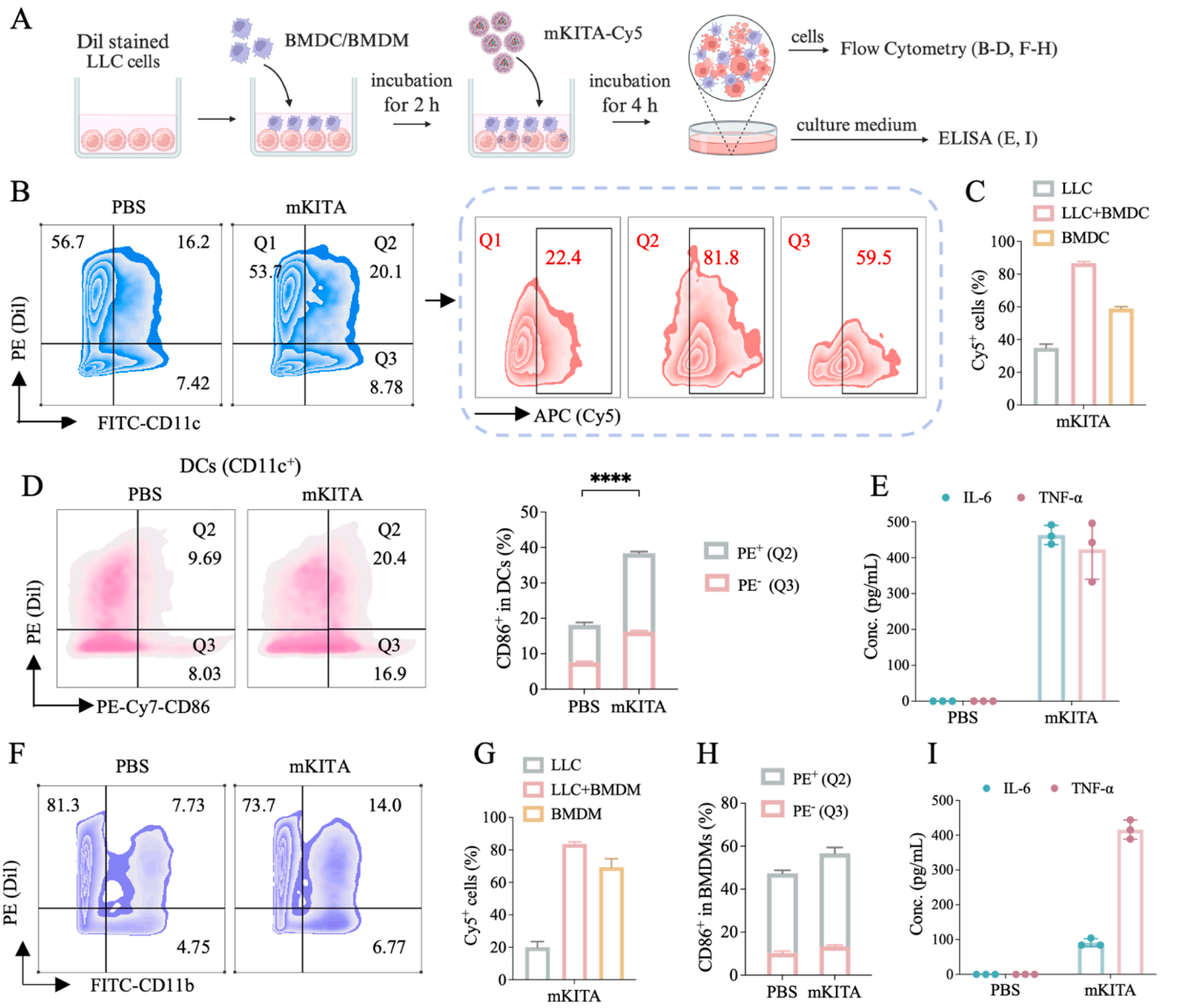

Fig. 3. Competitive uptake of Cy5-labeled mKITA by DIL-stained LLC cells and CD11c or CD11b stained APCs and the activation of immune cells (Cy5: 0.7 μM, n = 3). (A) Experimental flow. (B) Flow cytometric diagram and (C) proportions of endocytosis of mKITA, and (D) proportions of $CD86^+$ in BMDCs and (E) secretion of IL-6 and TNF-α in the co-culture of LLC cells and BMDCs at 4 h incubation. (F) Flow cytometric diagram and (G) proportions of endocytosis of mKITA, (H) proportions of $CD86^+$ in BMDM and (I) secretion of IL-6 and TNF-α in the co-culture of LLC cells and BMDM at 4 h incubation.

well tolerated, no significant body weight loss observed throughout the course of therapy (Fig. 5**B**), corroborating the favorable safety profile of the micellar platform. mKI or mTA monotherapies only marginally prolonged median survival times (MST: 17 or 19 days), showing outcomes similar to those in PBS group. Remarkably, mKITA group exhibited a doubling of MST to 29 days, highlighting the potent in vivo antitumor effects and therapeutic advantage conferred by the co-delivery strategy. To elucidate the mechanism underlying the high therapeutic efficacy, a biodistribution study of Cy5-labeled mKITA in orthotopic LLC tumor-bearing mice was conducted. Following i.v. administration, the micelles exhibited rapid and substantial accumulation in the tumorous lung tissue within 2 h (**Fig. S7**), consistent with previous reports [18,19]. This, coupled with systemic distribution achieved via i.v. delivery, enables targeting of both primary orthotopic tumors and any disseminated metastatic lesions, which is essential for eliciting a potent abscopal effect and durable adaptive immune response.

Most notably, mKITA+αPD-1 therapy led to durable responses, with 60% of animals' long-term tumor-free, demonstrating a profound synergistic benefit (Fig. 5**C**). The timing of αPD-1 administration followed the rationale of "prime-and-attack" strategy: in priming phase (e.g., days 3, 5, 7), mKITA remodeled the TME by inducing TAAs; and in attack phase, αPD-1 therapy (starting on day 8) sustained the T-cell inhibition during this optimal "therapeutic window" created by mKITA. This result is consistent with recent studies highlighting that targeted inhibition of the KRAS pathway can remodel TME and sensitize tumors to immune checkpoint therapy by promoting T cell infiltration and function [10]. Therefore, the potentiation of αPD-1 efficacy observed is likely attributable to increased $PD1^+$T cell frequencies and decreased adaptive resistance mechanisms following KRAS inhibition, as well as enhanced antigen presentation induced by mKITA.

Further mechanistic analyses using flow cytometry substantiated that mKITA treatment significantly reduced tumor cells ($CD45^-EpCAM^-CD31^-$) burden in lung tissue (Fig. 5**D-E**). Moreover, mKITA+αPD-1 group demonstrated a significant 4.3-fold reduction in PD-L1 expression on tumor cells (Fig. 5**F**), thus amplifying the suppression of the PD-

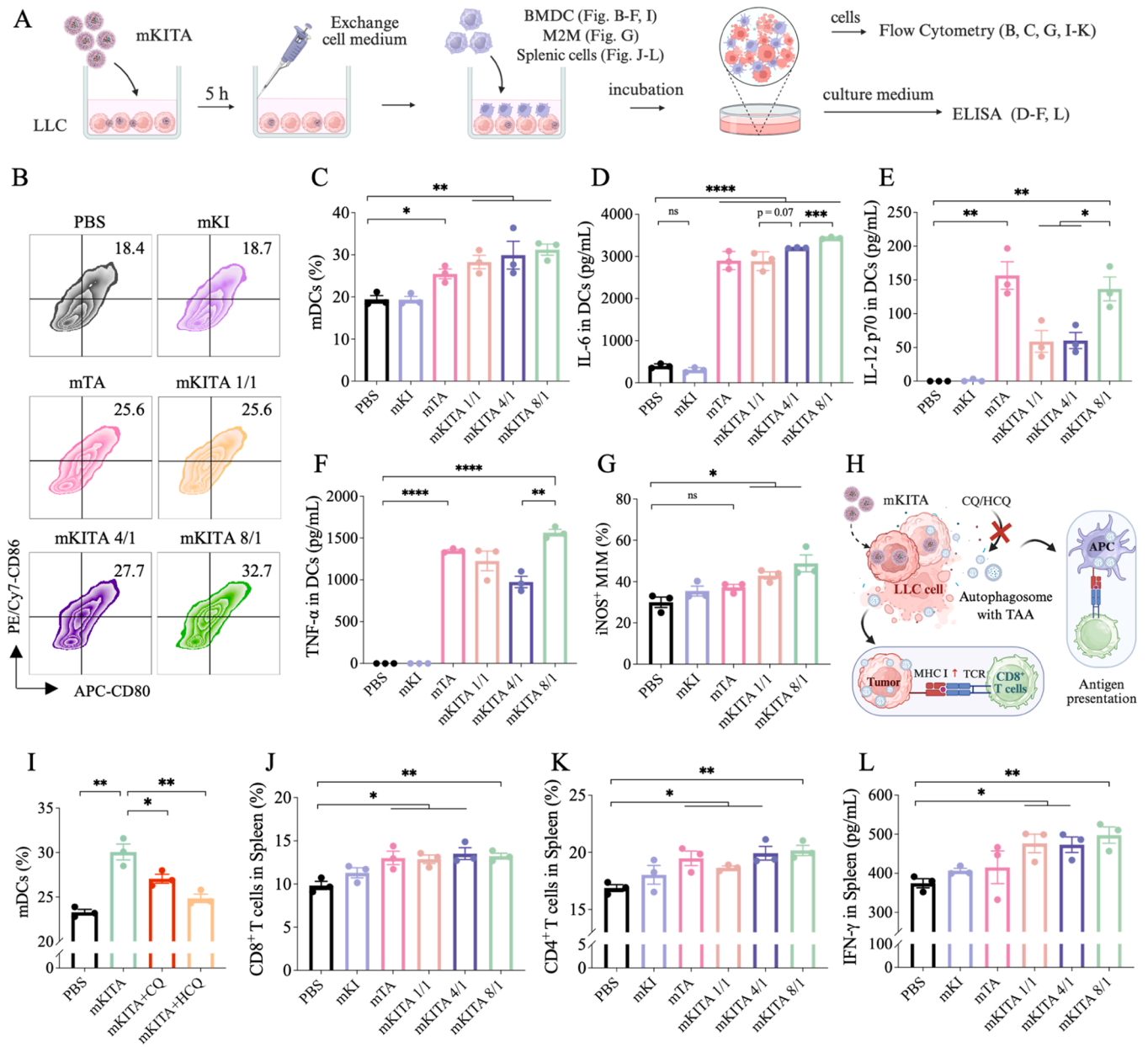

Fig. 4. Activation of immune cells by co-culturing with mKITA pretreated LLC cells (n = 3). (A) Experimental flow. (B) Flow cytometric diagrams and (C) proportions of mDCs, secretion of (D) IL-6, (E) IL-12, (F) TNF-α, as well as (G) proportions of iNOS^{+}M1M of IL-4-stimulated RAW264.7 cells at 8 h incubation with mKITA pretreated LLC cells. (H) Schematic diagram and (I) influence on the percentages of mDCs in the co-culture of BMDCs and LLC cells that were pretreated with mKITA and autophagy inhibitors. Proportions of (J) CD8^{+}T and (K) CD4^{+}T cells, and (L) secretion of IFN-γ of splenic cells at 24 h co-culture with mKITA pretreated LLC cells. * $p < 0.05$, ** $p < 0.01$, *** $p < 0.001$ and **** $p < 0.0001$.

1/PD-L1 immune checkpoint axis and enhancing the likelihood of durable immune-mediated tumor control. These data firmly demonstrate that mKITA not only achieves direct and immunogenic eradication of KRAS-mutant tumor, but also synergistically cooperates with checkpoint inhibition to overcome immune resistance and induce long-term tumor remission. This strategy sets the stage for combinatorial nanomedicine approaches aimed at addressing the therapeutic bottlenecks in the treatment of KRAS-driven malignancies.

3.8. Immunological mechanisms underlying the potent mKITA-based therapies in LLC model

To elucidate the mechanisms underlying the potent and durable antitumor immune efficacy observed with mKITA-based regimens, we conducted comprehensive immunophenotyping in the orthotopic LLC models (Fig. 5**D**) using gating strategies shown in **Fig. S8**. Analysis of the pulmonary TME revealed that nanoformulations markedly augmented the infiltration of total DCs and mDCs, in line with its in situ vaccine effect and capacity to amplify antigen presentation (**Figs. S9A,**5**G**). Concurrently, mKITA significantly remodeled the immunosuppressive niche, exemplified by a substantial reduction in M2M, which was further magnified by combination with αPD-1, reducing M2M abundance to only 15% of PBS group and raising the M1/M2 ratio from 0.77 to 1.22 (Figs. 5**H, S9B**). Notably, combination therapy also drove a twofold expansion of NK cells (**Fig. S9C**), reinforcing the critical engagement of the innate immune arm. The mKITA+αPD-1 therapy orchestrated the convergence of innate and adaptive immunity, as showed by enhanced recruitment of T cells to the lung (Figs. **S9D-F,**5**I-J**), achieving an 8.2-fold increase in IFN-γ^{+} cytotoxic T lymphocytes (CTLs) and 8.8-fold increase in IFN-γ^{+}Th1 cells. It is reported that IFN-γ upregulates the

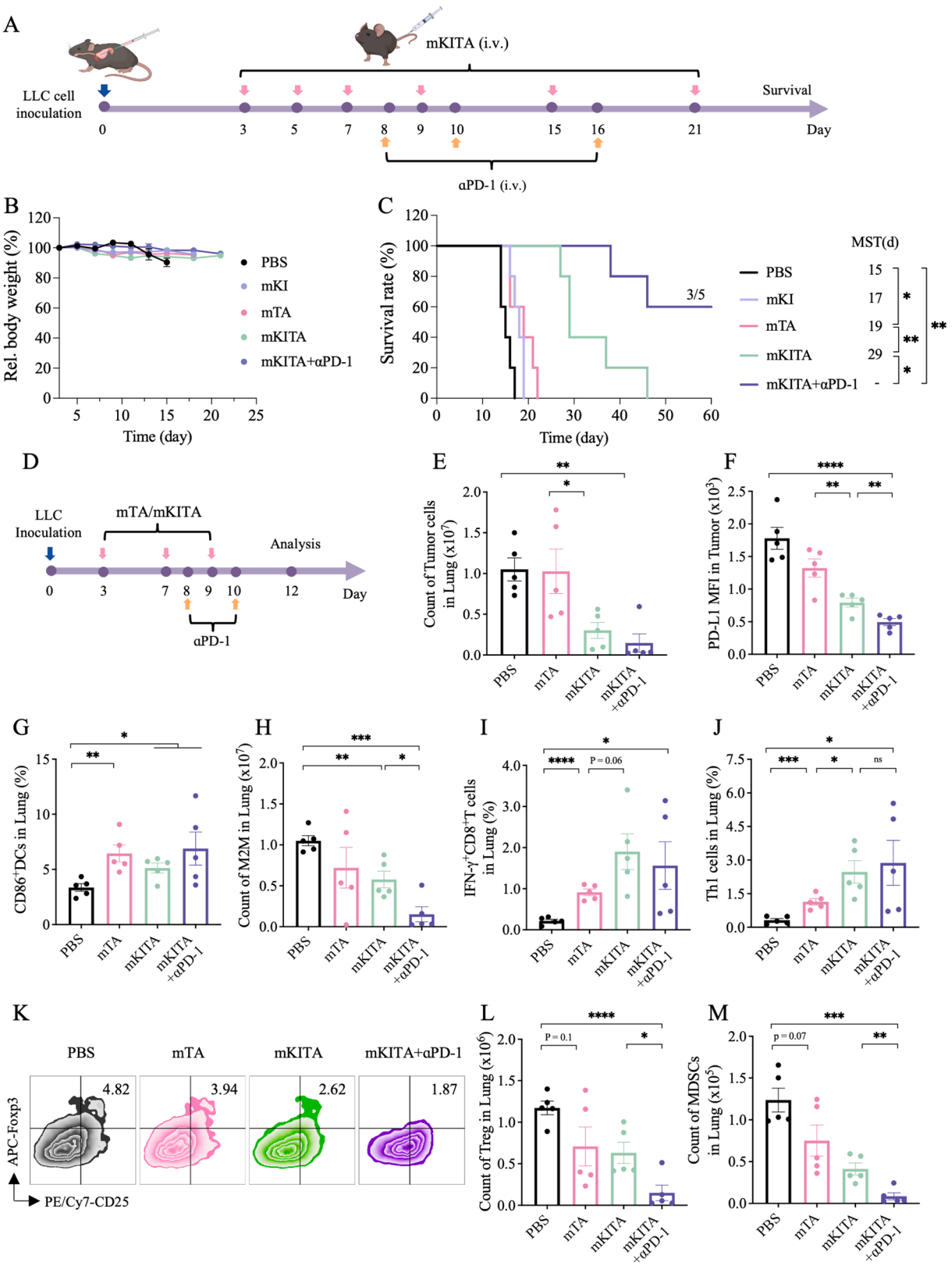

Fig. 5. Therapeutic efficacy of mKITA and its combination with αPD-1 on orthotopic LLC tumor models and lung TME analysis (KI: 16 mg/kg, TA: 1 mg/kg, αPD-1: 10 μg/mouse, n = 5). (A) Experimental workflow for efficacy, (B) body weight and (C) survival rates of the mice. (D) Experimental workflow for lung TME analysis in figures E-M. (E) Counts of LLC cells and (F) their surface expression of PD-L1. (G) Percentages of $CD86^{+}$DCs, (H) counts of M2M, and percentages of (I) IFN-$\gamma^{+}CD8^{+}$T cells and (J) Th1 cells. (K) Flow cytometric proportions and (L) counts of Tregs. (M) Counts of MDSCs in the lung tissue. * $p < 0.05$, ** $p < 0.01$, *** $p < 0.001$ and **** $p < 0.0001$.

expression of MHC I and enhances CTL-mediated recognition of tumor cells, meanwhile Th1 cells augment antitumor immune responses by secreting IFN-γ and TNF-α to facilitate $CD8^+$T cell activation [39,40]. In parallel, this regimen significantly reduced immunosuppressive Tregs and MDSCs within tumor (Fig. 5**K-M**). The heat map of immune cells exhibited a mutual transformation of the immunosuppressive TME of KRAS-mutant lung cancer toward a pro-inflammatory, anti-tumor state (**Fig. S9F**).

Effective and lasting tumor control further depends on systemic immune activation in lymphoid tissues/organs. In the spleen, mKITA-based therapies, particularly mKITA+αPD-1, significantly elevated the proportions of total DCs, MHC II^+ mDCs ($CD80^+CD86^+$MHC II^+) and IFN-I-producing pDCs ($CD11c^+B220^+$) (**Figs. S10A,** 6A, B), both being crucial for orchestrating tumor antigen recognition and cross-presentation. Notably, mKITA+αPD-1 induced a substantial expansion of B cells (to 49.4%, with significantly more activated $CD69^+$B cells; Fig. 6**C, D**), recruitment of NK cells (1.5-fold increase; **Fig. S10B**), and amplification of anti-tumor CTL and Th1 cell responses (Figs. 6**E-H, S10C-E**) with concomitant decrease in immunosuppressive MDSCs (**Fig. S10F**), thereby mounting a multi-dimensional immune response. Additionally, the observed elevations in anti-KRAS G12C and anti-WT1 antibody titers illustrated the capacity of this strategy to enable humoral and cellular synergy and epitope spreading (Fig. 6**I, J**). WT1 is well recognized as correlates of clinically favorable outcomes in NSCLC [41]. The epitope spreading indicates that the initial immune response targeting the primary antigens has successfully amplified into a broader, polyclonal attack against the tumor, thereby reducing tumor immune escape through antigen loss variants and enhancing the durability of anti-tumor immunity. Additionally, H&E staining images showed no inflammatory infiltration or necrosis in the major organs of the treated mice, indicating the biosafety and the absence of obvious systemic toxicity of mKITA therapy (**Fig. S11**).

These data are summarized in **Figs. S9G** and 6**K** illustrating the major effects of mKITA and its combination with αPD-1. mKITA have great impact on reducing MDSCs while simultaneously recruiting mDCs to activate IFN-γ^+CTLs and Th1 cells as well as humoral immunity. Beyond above effects, mKITA+αPD-1 elicits a broad-spectrum multi-layered immune response: further decreased M2M, Tregs and MDSCs,

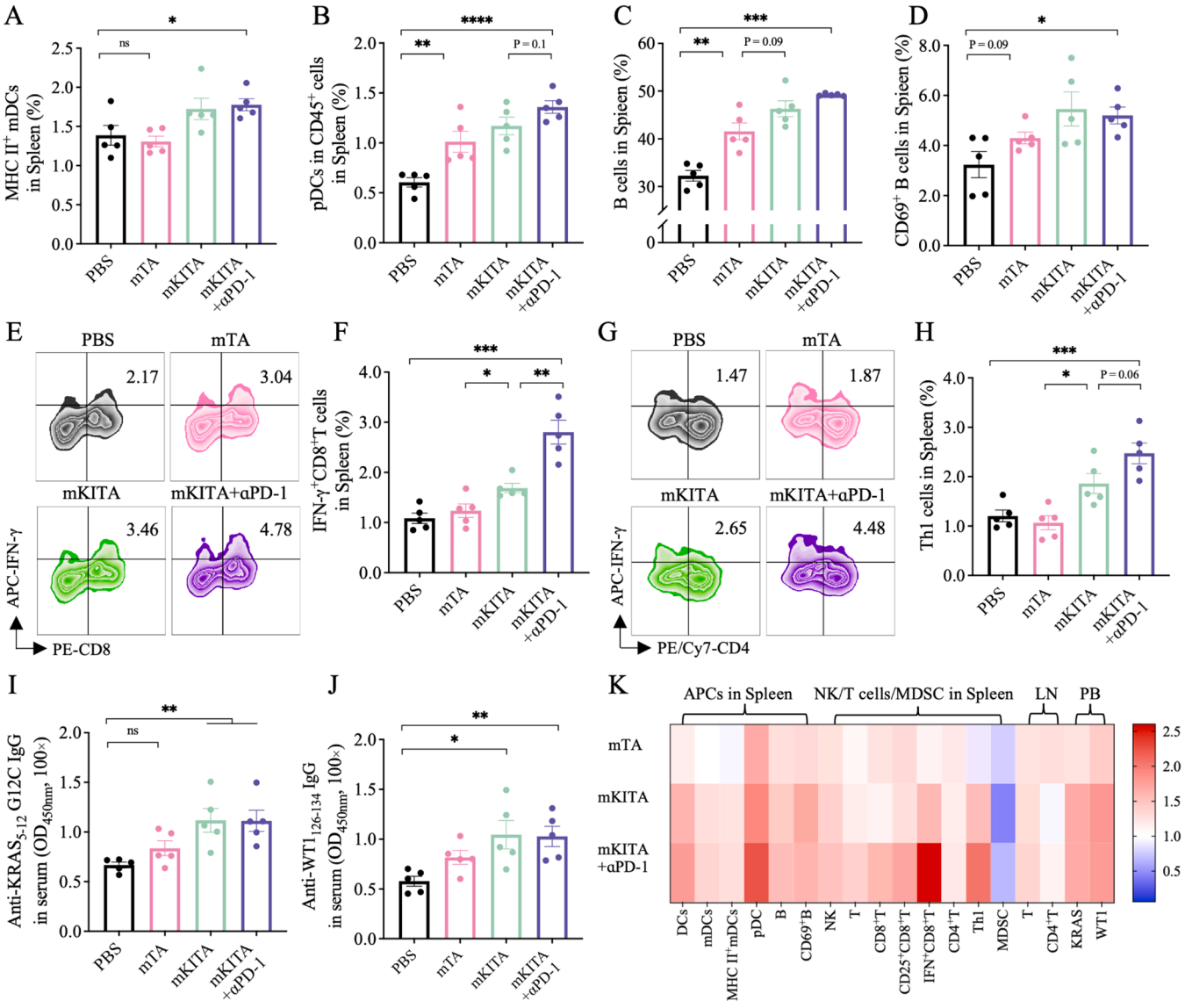

Fig. 6. Systemic immune analysis of orthotopic LLC tumor models treated with mKITA or mKITA+αPD-1 as in Fig. 5D (n = 5). Percentages of (A) MHC $II^+CD86^+CD80^+$DCs, (B) pDCs, (C) B cells and (D) $CD69^+$B cells in the spleen. (E) Flow cytometric diagrams and (F) percentages of IFN-γ^+CD8^+T cells, (G) flow cytometric diagrams and (H) percentages of Th1 cells in the spleen. Antibody titers against (I) KRAS G12C and (J) WT1 in peripheral blood. (K) Heat map of systemic immunity profiling results. * $p < 0.05$, ** $p < 0.01$, *** $p < 0.001$ and **** $p < 0.0001$.

significantly increased DCs, mDCs and pDCs, $CD8^+$T cells and their functional subsets IFN-γ^+CTLs and Th1 cells, broadening the scope of tumor antigen recognition and facilitating durable immune surveillance. This orchestrated immune remodeling highlights the translational promise of this reduction-sensitive co-delivery nano-platform combined with immunotherapy for overcoming resistance and establishing long-term control in hard-to-treat KRAS-mutant cancers.

4. Conclusion

In this study, we demonstrated that the mKITA nanoplatform through co-delivery of KRAS G12C inhibitor and TLR7/8 agonist, achieves potent and durable antitumor immunity in KRAS-mutant lung cancer. By leveraging enhanced tumor cell autophagy, ICD and in situ antigen release, combined with the localized and systemic activation of DCs, mKITA elicits potent in situ vaccine effect. This induces robust, multifaceted immune responses, including enhanced cross-presentation, expansion of IFN-γ^+ cytotoxic T cells and Th1 cells, and the generation of tumor-specific antibodies, with effective disruption of immunosuppressive networks within TME. mKITA nanoplatform overcomes the limitations of conventional in situ vaccines and holds translational potential for systemic administration and combination immunotherapy in solid tumors. When combined with PD-1 antibody, mKITA elicits higher tumor regression and long-term survival in 60% of LLC mice. This combinatorial approach surpasses the limitations of monotherapies and directly addresses key challenges in treating KRAS-driven and immunologically “cold” tumors, namely resistance development and lack of durable immune activation. The overall results suggest this approach as a translatable nano-enabled, immune-modulatory cancer therapy, wherein the integration of precise molecular targeting with microenvironmental and systemic immune reprogramming achieves robust therapeutic synergy. These findings establish a novel therapy that concurrently targets oncogenic KRAS signaling while overcoming multiple layers of immune suppression in the tumor microenvironment.

CRediT authorship contribution statement

Shiyu Miao: Writing – original draft, Methodology, Investigation, Formal analysis, Data curation. **Yinping Sun:** Methodology, Formal analysis, Data curation. **Yanyi Qu:** Methodology, Investigation, Formal analysis. **Luying Zhu:** Investigation, Formal analysis. **Zhiyuan Zhong:** Writing – review & editing, Supervision, Resources. **Fenghua Meng:** Writing – review & editing, Validation, Supervision, Project administration, Funding acquisition, Conceptualization.

Declaration of competing interest

The authors declare that they have no known competing financial interests or personal relationships that could have appeared to influence the work reported in this paper.

Acknowledgements

This work is supported by research grants from the National Key Research and Development Program of China (2024YFA1210303) and the National Natural Science Foundation of China (NSFC 52473142, 52033006). The authors thank Biorender.com for assisting with the illustrations (https://BioRender.com/s01f741).

Supplementary materials

Supplementary material associated with this article can be found, in the online version, at doi:10.1016/j.actbio.2025.12.045.

References

[1] J.H. Cook, G.E.M. Melloni, D.C. Gulhan, P.J. Park, K.M. Haigis, The origins and genetic interactions of KRAS mutations are allele- and tissue-specific, Nat. Commun. 12 (1) (2021) 1808, https://doi.org/10.1038/s41467-021-22125-z.
[2] A.D. Cox, S.W. Fesik, A.C. Kimmelman, J. Luo, C.J. Der, Drugging the undruggable RAS: mission possible? Nat. Rev. Drug Discov. 13 (11) (2014) 828–851, https://doi.org/10.1038/nrd4389.
[3] K.P. Papadopoulos, S.H.I. Ou, M.L. Johnson, J. Christensen, K. Velastegui, D. Potvin, D. Faltaos, R.C. Chao, A phase I/II multiple expansion cohort trial of MRTX849 in patients with advanced solid tumors with KRAS G12C mutation, J. Clin. Oncol. 37 (15) (2019), https://doi.org/10.1200/JCO.2019.37.15_suppl.TPS3161. TPS3161.
[4] M. Reck, D.P. Carbone, M. Garassino, F. Barlesi, Targeting KRAS in non-small-cell lung cancer: recent progress and new approaches, Ann. Oncol. 32 (9) (2021) 1101–1110, https://doi.org/10.1016/j.annonc.2021.06.001.
[5] M.M. Awad, S. Liu, I.I. Rybkin, K.C. Arbour, J. Dilly, V.W. Zhu, M.L. Johnson, R. S. Heist, T. Patil, G.J. Riely, J.O. Jacobson, X. Yang, N.S. Persky, D.E. Root, K. E. Lowder, H. Feng, S.S. Zhang, K.M. Haigis, Y.P. Hung, L.M. Sholl, B.M. Wolpin, J. Wiese, J. Christiansen, J. Lee, A.B. Schrock, L.P. Lim, K. Garg, M. Li, L. D. Engstrom, L. Waters, J.D. Lawson, P. Olson, P. Lito, S.I. Ou, J.G. Christensen, P. A. Janne, A.J. Aguirre, Acquired resistance to KRAS(G12C) inhibition in cancer, N. Engl. J. Med. 384 (25) (2021) 2382–2393, https://doi.org/10.1056/NEJMoa2105281.
[6] Y. Zhao, Y.R. Murciano-Goroff, J.Y. Xue, A. Ang, J. Lucas, T.T. Mai, F. Da Cruz Paula A, A.Y. Saiki, D. Mohn, P. Achanta, A.E. Sisk, K.S. Arora, R.S. Roy, D. Kim, C. Li, L.P. Lim, M. Li, A. Bahr, B.R. Loomis, E. de Stanchina, J.S. Reis-Filho, B. Weigelt, M. Berger, G. Riely, K.C. Arbour, J.R. Lipford, B.T. Li, P. Lito, Diverse alterations associated with resistance to KRAS(G12C) inhibition, Nature 599 (7886) (2021) 679–683, https://doi.org/10.1038/s41586-021-04065-2.
[7] T. Isermann, C. Sers, C.J. Der, B. Papke, KRAS inhibitors: resistance drivers and combinatorial strategies, Trends Cancer 11 (2) (2025) 91–116, https://doi.org/10.1016/j.trecan.2024.11.009.
[8] Y. Adachi, K. Ito, Y. Hayashi, R. Kimura, T.Z. Tan, R. Yamaguchi, H. Ebi, Epithelial-to-mesenchymal transition is a cause of both intrinsic and acquired resistance to KRAS G12C inhibitor in KRAS G12C-mutant non-small cell lung cancer, Clin. Cancer Res. 26 (22) (2020) 5962–5973, https://doi.org/10.1158/1078-0432.Ccr-20-2077.
[9] J. Canon, K. Rex, A.Y. Saiki, C. Mohr, K. Cooke, D. Bagal, K. Gaida, T. Holt, C. G. Knutson, N. Koppada, B.A. Lanman, J. Werner, A.S. Rapaport, T. San Miguel, R. Ortiz, T. Osgood, J.R. Sun, X. Zhu, J.D. McCarter, L.P. Volak, B.E. Houk, M. G. Fakih, B.H. O’Neil, T.J. Price, G.S. Falchook, J. Desai, J. Kuo, R. Govindan, D. S. Hong, W. Ouyang, H. Henary, T. Arvedson, V.J. Cee, J.R. Lipford, The clinical KRAS(G12C) inhibitor AMG 510 drives anti-tumour immunity, Nature 575 (7781) (2019) 217–223, https://doi.org/10.1038/s41586-019-1694-1.
[10] E. Mugarza, F. van Maldegem, J. Boumelha, C. Moore, S. Rana, M. Llorian Sopena, P. East, R. Ambler, P. Anastasiou, P. Romero-Clavijo, K. Valand, M. Cole, M. Molina-Arcas, J. Downward, Therapeutic KRAS(G12C) inhibition drives effective interferon-mediated antitumor immunity in immunogenic lung cancers, Sci. Adv. 8 (29) (2022) eabm8780, https://doi.org/10.1126/sciadv.abm8780.
[11] M. Molina-Arcas, J. Downward, Exploiting the therapeutic implications of KRAS inhibition on tumor immunity, Cancer Cell 42 (3) (2024) 338–357, https://doi.org/10.1016/j.ccell.2024.02.012.
[12] C. Zuany-Amorim, J. Hastewell, C. Walker, Toll-like receptors as potential therapeutic targets for multiple diseases, Nat. Rev. Drug Discov. 1 (10) (2002) 797–807, https://doi.org/10.1038/nrd914.
[13] A.H. Rook, J.C. Gelfand, M. Wysocka, A.B. Troxel, B. Benoit, C. Surber, R. Elenitsas, M.A. Buchanan, D.S. Leahy, R. Watanabe, I.R. Kirsch, E.J. Kim, R.A. Clark, Topical resiquimod can induce disease regression and enhance T-cell effector functions in cutaneous T-cell lymphoma, Blood 126 (12) (2015) 1452–1461, https://doi.org/10.1182/blood-2015-02-630335.
[14] P.J. Pockros, D. Guyader, H. Patton, M.J. Tong, T. Wright, J.G. McHutchison, T. C. Meng, Oral resiquimod in chronic HCV infection: safety and efficacy in 2 placebo-controlled, double-blind phase IIa studies, J. Hepatol. 47 (2) (2007) 174–182, https://doi.org/10.1016/j.jhep.2007.02.025.
[15] R.R. Khusnutdinov, Could drug delivery systems be enhancers for therapy against KRAS-driven cancers? Rev. Adv. Chem. 14 (2025) 273–304, https://doi.org/10.1134/S2634827624600312.
[16] Y. Mei, X. Qin, Z. Yang, S. Song, X. Liu, C. Wu, J. Qian, X. Huang, Y. Zhang, W. He, Engineered a dual-targeting HA-TPP/A nanoparticle for combination therapy against KRAS-TP53 co-mutation in gastrointestinal cancers, Bioact. Mater. 32 (2024) 277–291, https://doi.org/10.1016/j.bioactmat.2023.10.003.
[17] S. Bhagchandani, J.A. Johnson, D.J. Irvine, Evolution of toll-like receptor 7/8 agonist therapeutics and their delivery approaches: from antiviral formulations to vaccine adjuvants, Adv. Drug Deliv. Rev. 175 (2021) 113803, https://doi.org/10.1016/j.addr.2021.05.013.
[18] W. Yan, B. Guo, Z. Wang, J. Yang, Z. Zhong, F. Meng, RGD-directed 24 nm micellar docetaxel enables elevated tumor-liver ratio, deep tumor penetration and potent suppression of solid tumors, J. Control Release 360 (2023) 304–315, https://doi.org/10.1016/j.jconrel.2023.06.032.
[19] D. Ni, B. Guo, Z. Zhong, Y. Chen, G. Yang, J. Yang, Z. Zhong, F. Meng, Integrin-targeting disulfide-crosslinked micellar docetaxel eradicates lung and prostate cancer patient-derived xenografts, Acta Biomater. 170 (2023) 228–239, https://doi.org/10.1016/j.actbio.2023.08.043.
[20] C.B. Rodell, S.P. Arlauckas, M.F. Cuccarese, C.S. Garris, R. Li, M.S. Ahmed, R. H. Kohler, M.J. Pittet, R. Weissleder, TLR7/8-agonist-loaded nanoparticles

promote the polarization of tumour-associated macrophages to enhance cancer immunotherapy, Nat. Biomed. Eng. 2 (8) (2018) 578–588, https://doi.org/10.1038/s41551-018-0236-8.
[21] K. Benderski, T. Lammers, A.M. Sofias, Analysis of multi-drug cancer nanomedicine, Nat. Nanotechnol. 20 (8) (2025) 1163–1172, https://doi.org/10.1038/s41565-025-01932-1.
[22] J. Wang, W. Mao, L.L. Lock, J. Tang, M. Sui, W. Sun, H. Cui, D. Xu, Y. Shen, The role of micelle size in tumor accumulation, penetration, and treatment, ACS Nano 9 (7) (2015) 7195–7206, https://doi.org/10.1021/acsnano.5b02017.
[23] J.X. Li, R.Z. Li, A. Sun, H. Zhou, E. Neher, J.S. Yang, J.M. Huang, Y.Z. Zhang, Z. B. Jiang, T.L. Liang, L.R. Ma, J. Wang, X.R. Wang, X.Q. Fan, J. Huang, Y. Xie, L. Liu, L. Tang, E.L.H. Leung, P.Y. Yan, Metabolomics and integrated network pharmacology analysis reveal tricin as the active anti-cancer component of weijing decoction by suppression of PRKCA and sphingolipid signaling, Pharmacol. Res. 171 (2021) 105574, https://doi.org/10.1016/j.phrs.2021.105574.
[24] T.C. Chou, Theoretical basis, experimental design, and computerized simulation of synergism and antagonism in drug combination studies, Pharmacol. Rev. 58 (3) (2006) 621–681, https://doi.org/10.1124/pr.58.3.10.
[25] J. Dai, L. Fang, X. Wang, J. Hua, Y. Tu, S. Li, K. He, L. Hang, Y. Xu, J. Fang, L. Wang, J. Wang, P. Ma, G. Jiang, Configuration-mediated efficient non-radiative transition for R848-assisted photothermal immunotherapy to inhibit tumor growth and metastasis by an in situ tumor vaccine strategy, Angew. Chem. Int. Ed. Engl. 64 (6) (2025) e202417871, https://doi.org/10.1002/anie.202417871.
[26] J.J. Rennick, A.P.R. Johnston, R.G. Parton, Key principles and methods for studying the endocytosis of biological and nanoparticle therapeutics, Nat. Nanotechnol. 16 (3) (2021) 266–276, https://doi.org/10.1038/s41565-021-00858-8.
[27] P.A. Janne, G.J. Riely, S.M. Gadgeel, R.S. Heist, S.I. Ou, J.M. Pacheco, M. L. Johnson, J.K. Sabari, K. Leventakos, E. Yau, L. Bazhenova, M.V. Negrao, N. A. Pennell, J. Zhang, K. Anderes, H. Der-Torossian, T. Kheoh, K. Velastegui, X. Yan, J.G. Christensen, R.C. Chao, A.I. Spira, Adagrasib in non-small-cell lung cancer harboring a $KRAS^{G12C}$ mutation, N. Engl. J. Med. 387 (2) (2022) 120–131, https://doi.org/10.1056/NEJMoa2204619.
[28] K.L. Bryant, C.A. Stalnecker, D. Zeitouni, J.E. Klomp, S. Peng, A.P. Tikunov, V. Gunda, M. Pierobon, A.M. Waters, S.D. George, G. Tomar, B. Papke, G.A. Hobbs, L. Yan, T.K. Hayes, J.N. Diehl, G.D. Goode, N.V. Chaika, Y.X. Wang, G.F. Zhang, A. K. Witkiewicz, E.S. Knudsen, E.F. Petricoin, P.K. Singh, J.M. Macdonald, N.L. Tran, C.A. Lyssiotis, H.Q. Ying, A.C. Kimmelman, A.D. Cox, C.J. Der, Combination of ERK and autophagy inhibition as a treatment approach for pancreatic cancer, Nat. Med. 25 (4) (2019) 628–640, https://doi.org/10.1038/s41591-019-0368-8.
[29] D.J. Klionsky, A.K. Abdel-Aziz, S. Abdelfatah, M. Abdellatif, A. Abdoli, S. Abel, et al., Guidelines for the use and interpretation of assays for monitoring autophagy, Autophagy 17 (1) (2021) 1–382, https://doi.org/10.1080/15548627.2020.1797280.
[30] J.P. Yang, Z.L. Yang, H. Wang, Y.C. Chang, J.F. Xu, X. Zhang, A polymeric nanoparticle to co-deliver mitochondria-targeting peptides and Pt(IV) prodrug: toward high loading efficiency and combination efficacy, Angew. Chem. Int. Ed. 63 (18) (2024) e202402291, https://doi.org/10.1002/anie.202402291.
[31] E. Terraza-Silvestre, R. Villamuera, J. Bandera-Linero, M. Letek, D. Oña-Sánchez, C. Ramón-Barros, C. Moyano-Jimeno, F.X. Pimentel-Muiños, An unconventional autophagic pathway that inhibits ATP secretion during apoptotic cell death, Nat. Commun. 16 (1) (2025) 3409, https://doi.org/10.1038/s41467-025-58619-3.
[32] H. Xia, D.R. Green, W. Zou, Autophagy in tumour immunity and therapy, Nat. Rev. Cancer 21 (5) (2021) 281–297, https://doi.org/10.1038/s41568-021-00344-2.
[33] W. Gao, X. Wang, Y. Zhou, X. Wang, Y. Yu, Autophagy, ferroptosis, pyroptosis, and necroptosis in tumor immunotherapy, Signal Transduct. Target. Ther. 7 (1) (2022) 196, https://doi.org/10.1038/s41392-022-01046-3.
[34] L. Galluzzi, E. Guilbaud, D. Schmidt, G. Kroemer, F.M. Marincola, Targeting immunogenic cell stress and death for cancer therapy, Nat. Rev. Drug Discov. 23 (6) (2024) 445–460, https://doi.org/10.1038/s41573-024-00920-9.
[35] Q. Ma, W. Zhang, K. Wu, L. Shi, The roles of KRAS in cancer metabolism, tumor microenvironment and clinical therapy, Mol. Cancer 24 (1) (2025) 14, https://doi.org/10.1186/s12943-024-02218-1.
[36] S. Gerstberger, Q. Jiang, K. Ganesh, Metastasis, Cell 186 (8) (2023) 1564–1579, https://doi.org/10.1016/j.cell.2023.03.003.
[37] V. Turco, K. Pfleiderer, J. Hunger, N.K. Horvat, K. Karimian-Jazi, K. Schregel, M. Fischer, G. Brugnara, K. Jähne, V. Sturm, Y. Streibel, D. Nguyen, S. Altamura, D. A. Agardy, S.S. Soni, A. Alsasa, T. Bunse, M. Schlesner, M.U. Muckenthaler, R. Weissleder, W. Wick, S. Heiland, P. Vollmuth, M. Bendszus, C.B. Rodell, M. O. Breckwoldt, M. Platten, T cell-independent eradication of experimental glioma by intravenous TLR7/8-agonist-loaded nanoparticles, Nat. Commun. 14 (1) (2023) 771, https://doi.org/10.1038/s41467-023-36321-6.
[38] V. Hornung, S. Rothenfusser, S. Britsch, A. Krug, B. Jahrsdorfer, T. Giese, S. Endres, G. Hartmann, Quantitative expression of toll-like receptor 1-10 mRNA in cellular subsets of human peripheral blood mononuclear cells and sensitivity to CpG oligodeoxynucleotides, J. Immunol. 168 (9) (2002) 4531–4537, https://doi.org/10.4049/jimmunol.168.9.4531.
[39] F. Castro, A.P. Cardoso, R.M. Gonçalves, K. Serre, M.J. Oliveira, Interferon-gamma at the crossroads of tumor immune surveillance or evasion, Front. Immunol. 9 (2018) 847, https://doi.org/10.3389/fimmu.2018.00847.
[40] J. Borst, T. Ahrends, N. Babala, C.J.M. Melief, W. Kastenmuller, $CD4^{+}$T cell help in cancer immunology and immunotherapy, Nat. Rev. Immunol. 18 (10) (2018) 635–647, https://doi.org/10.1038/s41577-018-0044-0.
[41] M.A. Cheever, J.P. Allison, A.S. Ferris, O.J. Finn, B.M. Hastings, T.T. Hecht, I. Mellman, S.A. Prindiville, J.L. Viner, L.M. Weiner, L.M. Matrisian, The prioritization of cancer antigens: a national cancer institute pilot project for the acceleration of translational research, Clin. Cancer Res. 15 (17) (2009) 5323–5337, https://doi.org/10.1158/1078-0432.CCR-09-0737.